



Enhanced thermal performance of form-stable phase change materials with organic and inorganic supporting nanofillers

Wei-Chi Lai¹ · Ren-Wei Fan¹

Received: 5 February 2022 / Accepted: 2 November 2022 / Published online: 15 November 2022
© Akadémiai Kiadó, Budapest, Hungary 2022

Abstract

Organic phase change materials (PCMs) are inexpensive, safe, and do not segregate. However, they exhibit a low thermal conductivity. Several papers have reported the synthesis of organic–inorganic hybrid PCMs by adding inorganic fillers to increase the thermal conductivity. However, large amounts of fillers are needed to support the shape for the encapsulation of PCMs. Herein, we propose a facile synthesis strategy that yields composite PCMs with enhanced thermal performance. Initially, 1,3:2,4-dibenzylidene sorbitol (DBS) organogel was added as an organic filler to poly(ethylene glycol) (PEG) PCMs for maintaining the form and prevent leakage. Subsequently, a small amount of an inorganic filler, graphene nanoplatelets (GNPs), was added to these organic PCMs. Consequently, the thermal conductivity and shape stabilization of the PEG/GNPs/DBS PCMs were significantly improved. These prepared composite PCMs, with excellent shape stabilization, appropriate latent heat, and ideal thermal conductivity, are potential as fillers in solar-thermal systems and energy-efficient buildings.

Keywords Nanofibrils · Graphene nanoplatelet · Phase change material

Introduction

Recently, thermal energy storage has garnered significant attention because it allows the transfer and storage of thermal energy, reducing the overall energy demand. Latent heat thermal energy storage systems are the most common approaches owing to the associated high energy storage density and small temperature change during heat release; particularly, phase change materials (PCMs) are prevalently employed for latent heat thermal energy storage [1–3]. PCMs release or absorb latent heat during phase change process and are used in several applications such as building energy conservation, solar thermal energy, green textiles, and lithium-ion batteries [4–6].

PCMs are divided into three types: inorganic, organic, and eutectic organic and inorganic compounds [7, 8]. Inorganic PCMs exhibit excellent thermal conductivity but have several disadvantages including corrosion, supercooling, and lack of thermal stability. Contrastingly, organic PCMs have

no corrosive problems and do not show supercooling and phase segregation, but their thermal conductivity is low. As the drawbacks of inorganic PCMs are more critical than those of organic PCMs, the latter have attracted significant attention in recent years [9–12]. Organic PCMs involve linear long chain hydrocarbons, esters, and poly(ethylene glycol) (PEG). PEG is the most popular organic PCM [12] because it is non-flammable, inexpensive, and exhibits good latent heat. Therefore, PEG was chosen for this study.

The leakage of melted (liquid) PCMs leads to increased cost and thermal resistance [9]. Recently, several papers have reported the preparation of form-stable (also called shape-stabilized) PCMs to avoid the leakage problems; many synthesizing methods have been proposed, such as encapsulation, adsorbing or soaking porous material, and blending or copolymerization of polymers as supporting materials [13–16]. Belessiotis et al. investigated the preparation of shape-stabilized paraffin/SiO₂ composite PCMs using a chemically aided infiltration method [13]. The PCMs with 80 mass% paraffin exhibited the highest encapsulation ratio and latent heat of 156 J g⁻¹. Hasanabadi et al. employed the vacuum impregnation method to synthesize PCMs comprising paraffin/expanded perlite composites. The latent heat decreased around 18%; however, no significant leakage was observed [14].

✉ Wei-Chi Lai
wclai@mail.tku.edu.tw

¹ Department of Chemical and Materials Engineering,
Tamkang University, No.151, Yingzhuang Rd, Tamsui Dist,
New Taipei City 25137, Taiwan

The organic PCMs exhibit low thermal conductivity. Consequently, several studies have investigated the synthesis of organic–inorganic hybrid PCMs with added inorganic fillers to increase the thermal conductivity [17–24]. Generally, solid particles, such as metal particles, metal oxides, carbon nanofibers, carbon nanotubes, and graphene oxide (GO) or graphene nanoplatelets (GNPs), are dispersed into organic PCMs. However, large amounts of inorganic particles are required to support the shape imparted by the encapsulation of PCMs to prevent leakage. For example, Mehrali et al. reported an evident increase in the thermal conductivity of palmitic acid (PA) PCMs using GO as the supporting material [21]. However, approximately 50 mass% GO was required for enhancing the thermal conductivity. Lin et al. investigated the thermal properties of PA-composite PCMs for thermal energy storage. PCMs with 30 mass% SiO₂ demonstrated the least leakage percentage [24]. In addition, organic supporting fillers such as high-density polyethylene, polymethyl methacrylate, cellulose diacetate, and balsa wood have also been added to prevent leakage [25–28]. However, the thermal conductivities of these form-stable organic PCMs are lower, limiting their practical applications.

GNPs are nanoparticles consisting of stacks of graphene sheets and exhibit good physical properties for PCM applications. In comparison with carbon nanotubes or fibers, platelet-type structures exhibit a lower thermal contact resistance at low loads, yielding high thermal conductivity. Mehrali et al. reported an enhancement of thermal conductivity of PA PCMs by the addition of GNPs, which exhibited good thermal reliability after thermal cycling [22]. Yang et al. found the introduction of a small amount of GNPs into PEG/boron nitride (BN) PCMs for improving the thermal conductivity; the BN content ranged between 10 and 30 mass% [23].

A green and cheap organogelator, 1,3:2,4-dibenzylidene-D-sorbitol (DBS), was chosen as the main supporting material for the synthesis of novel form-stable composite PCMs. DBS is derived from the natural sugar-based amphiphiles with hydroxyl groups and phenyl rings. Notably, DBS (see Fig. 1) can self-assemble into three-dimensional networks with relatively small amounts in organic surroundings to produce organogels [29–31]. The mechanism underlying DBS network formation is controlled by the intermolecular hydrogen bonds of terminal hydroxyl groups and π interactions of phenyl rings between the DBS. The nearest hydrogen bonds and the most stable CH– π interactions are preferred for gel formation [29]. These DBS gel networks could significantly stabilize the shape by capturing melted PCMs during the phase change process. Although a few studies used organogel scaffolds to keep the shape [32, 33], the thermal conductivity of PCMs was not improved by adding the organic compound DBS. Therefore, in this study, high thermal conductivity

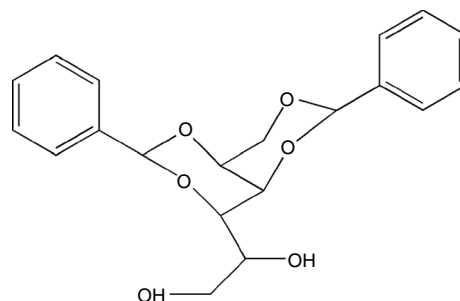


Fig. 1 Chemical structure of DBS

inorganic fillers, GNPs, were added to increase the thermal conductivity of composite PCMs. The contribution of this study is that we demonstrate that the addition of a large amount of inorganic fillers, which are usually expensive, is not necessary to provide shape support. Alternatively, a cheap and eco-friendly sorbitol derivative, DBS, can be mainly used as the organic supporting filler to maintain the form. These DBS nanofibrillar networks capture most of the melted PCMs and stabilize the shape against leakage. To the best of our knowledge, the preparation of composite PCMs with organic and inorganic supporting nanofillers has not been investigated yet.

In the present study, DBS was added to maintain the shape of PEG PCM. The self-assembled nanofibrillar networks with DBS captured most of the PCM, stabilizing the shape to prevent the leakage during the phase transitions. Subsequently, small amounts of inorganic GNPs were added to the PEG/DBS PCMs for improving the form stabilization and thermal conductivity. The fabricated PCMs with DBS and GNPs retained its shape up to 120 °C, exhibiting excellent shape stabilization. The thermal conductivity of the PCMs was 2.3 times larger than that obtained using organic PCMs. The resulting PCMs are potential candidates for applications in solar power plants, solar water heaters, air-based heating systems, and cooling/heating of buildings, where the temperature range is approximately 40–60 °C [34, 35].

Experimental

Materials

Poly (ethylene glycol) (PEG: 8000 g mole⁻¹) was obtained by Sigma-Aldrich. Graphene nanoplatelets (GNPs) were purchased from XG Sciences (Grade C: a specific surface area of 300 m² g⁻¹). The thickness of the GNPs was approximately 1–5 nm, as provided by the supplier.

1,3:2,4-Dibenzylidene-D-sorbitol (DBS) was purchased by Milliken Chemicals.

Sample preparation

Initially, PEG (2 g) and 7 mass% DBS were mixed at 250 °C under constant agitation for 10 min. When the DBS was completely dissolved in the PEG, varying amounts of GNP (0–8 mass%) were added to the PEG/DBS solutions and maintained at 250 °C under constant agitation for 30 min. Finally, the prepared PCMs were cooled to room temperature and were maintained for more than 24 h before the experiments.

Dynamic Rheological test

The rheological behaviors of the composite PCMs containing 0–8 mass% GNPs were analyzed using a Physica MCR 101 rheometer (Anton Paar). The amplitude sweep test was performed over a strain range of 0.05–5% with a frequency of 10 rad s⁻¹ at 25 °C. The frequency sweep test was performed between 0.1 and 800 rad s⁻¹ with a strain amplitude maintained at 0.1% at 25 °C. Gel dissolution temperatures (T_d) of the composite PCMs containing 0–8 mass% GNPs were calculated from elastic modulus G' versus temperature using the intersection of the tangents of the curves. The composite PCMs were heated from 80 to 150 °C with a heating rate of 5 °C min⁻¹. The strain amplitude was maintained at 0.1%, and the frequency was 10 rad s⁻¹.

Structure

The structures of the composite PCMs containing 0–8 mass% GNPs were investigated by a H-7100 transmission electron microscope (Hitachi). The composite PCMs for TEM were prepared by adding dropwise of molten samples onto the carbon-supported TEM grids and then were maintained in a vacuum oven at 25 °C for more than 24 h. Eventually, the composite PCMs were washed by deionized water and were kept inside a vacuum oven at 40 °C for 12 h.

Heating/cooling performance

The thermal performances of the composite PCMs containing 0–8 mass% GNPs were tested through Pyris Diamond differential scanning calorimeter (Perkin Elmer). The composite PCMs were heated from 0 to 100 °C with a heating rate of 5 °C min⁻¹, and the melting temperature (T_m) and latent heat of melting (ΔH_m) were observed. ΔH_m

can be determined from the integrating the area under the endothermic peak of the DSC curve. Subsequently, the composite PCMs were cooled from 100 to 0 °C with a cooling rate of 5 °C min⁻¹ under a nitrogen atmosphere, and the crystallization temperature (T_c) and latent heat of freezing (ΔH_c) were measured. ΔH_c was determined by integrating the area under the exothermic peak of the DSC curve.

Leakage measurement

The leakage tests of the composite PCMs containing 0–8 mass% GNPs were performed using the filter sheet sandwich method. The composite PCMs were heated to 250 °C for 5 min, and the molten PCMs were dripped onto a copper ring with a diameter of 1.5 cm and a thickness of 3 mm on a glass plate. The mass of the composite PCMs was 0.6 g. The copper ring was removed after the composite PCMs were cooled to room temperature. Subsequently, the composite PCMs were placed on a 2-mm square stainless-steel mesh (filter sheet) prior to the leakage test. The filter sheets were weighed before (M_1) and subsequent the annealing step (M_2). The composite PCMs were weighed at different temperatures above the PEG melting temperature at an interval of 30 min. The leakage percentage was calculated by Eq. (1):

$$\text{Leakage percentage(\%)} = \left[\frac{M_2 - M_1}{M_1} \right] \times 100 \quad (1)$$

Dimensional stability measurement

The dimensional stability measurements of the composite PCMs containing 0–8 mass% GNPs were measured using a Q400 thermomechanical analyzer (TA). The PCMs were heated from 25 to 100 °C at a heating rate of 3 °C min⁻¹, and the constant normal force was 0.01 N.

Thermal conductivity test

The thermal conductivities of the composite PCMs containing 0–8 mass% GNPs were measured using a KD-2 Pro Model thermal properties analyzer (Decagon Devices) at 25 °C; the measurements were repeated at least thrice. The composite PCMs (12 g) were heated at 200 °C for 5 min, poured into a 7-mL vial using the SH-1 dual needle probe sensor (1.3 mm diameter, 30 mm length, and 6 mm spacing), and then cooled to 25 °C in a water bath with a temperature error within ± 2 °C for more than 24 h. The needle was completely inserted into the 7-mL vial. The measuring thermal conductivity range of the sensor was 0.02–0.2 W m⁻¹ K⁻¹, and the read time was set to 2 min. The thermal conductivity of each composite PCM was measured at least five times.

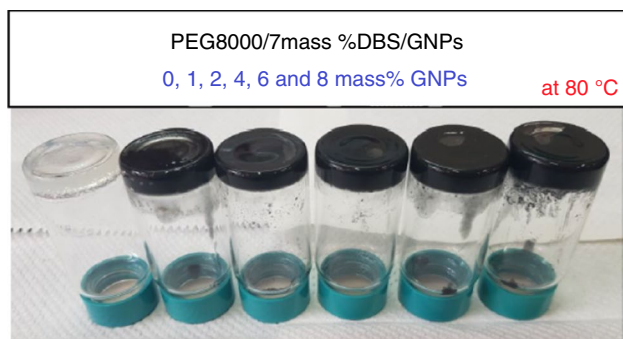


Fig. 2 Photographs of the composite PCMs containing 0–8 mass% GNP contents at 80 °C

Results and discussion

Phase behavior and rheological measurement

Figure 2 exhibits the photographs of the composite PCMs containing 0–8 mass% GNP contents at 80 °C, and is much higher than the PEG melting temperature (approximately 60 °C). A visual observation indicates the formation of transparent gels in the samples without GNPs, which may be attributed to the DBS gel network formation. The samples became translucent gels with the addition of GNPs. However, when the GNP content exceeded 8 mass%, the composite PCMs became heterogeneous, and precipitation occurred. The composite PCMs with 0–8 mass% GNPs were chosen for the subsequent investigations for the present study.

Rheometer was used to investigate the viscoelastic characteristics of the composite PCMs containing 0–8 mass% GNPs at high temperatures. Figure 3 displays the (a) G' versus strain, and (b) G' and G'' versus frequency) of the composite PCMs containing 0–8 mass% GNPs at 80 °C. G' did not show significant variation when the strain was below 0.5% (Fig. 3 a). However, it decreased significantly when the strain increased around 0.5%, indicating the structure started to destroy at the higher strain.

G' was always larger than G'' ; G'' and G'' did not significantly influence with frequency (Fig. 3 b), which suggests that the composite PCMs can be considered as gels. The results indicate that the masses of the PCM samples remain unchanged at 80 °C. Additionally, G' increased with an increase in the GNP concentration, suggesting an increase in the stiffness of the composite PCMs with increasing GNP content.

Figure 4 demonstrates the G' versus temperature of the composite PCMs containing 0–8 mass% GNPs. T_d values were calculated from the intersection of the tangents (see dashed line in Fig. 4); the composite PCMs started to exhibit liquid states beyond T_d . The values of T_d of the composite PCMs with 0, 1, 2, 4, 6, and 8 mass% GNPs were 119.1,

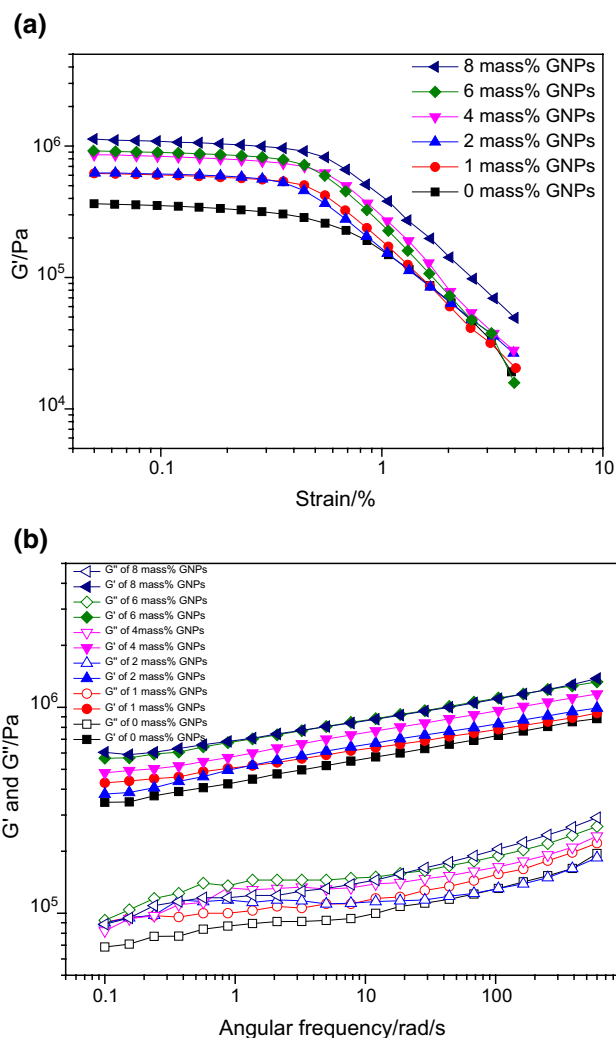


Fig. 3 a G' versus strain, and b G' and G'' versus frequency) of the composite PCMs containing 0–8 mass% GNPs at 80 °C

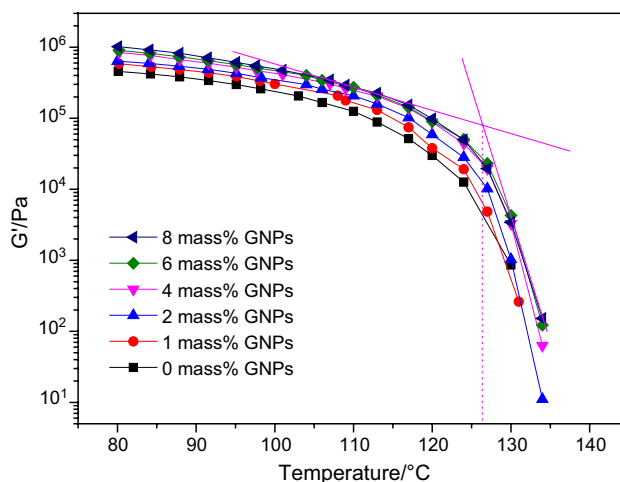


Fig. 4 G' versus temperature of the composite PCMs containing 0–8 mass% GNPs

123.0, 125.9, 126.2, 126.3, and 126.3 °C, respectively. These temperatures were significantly larger than the melting temperature of PEG (approximately 60 °C). The prepared composite PCMs retain their shape until the temperature is approximately two times the melting temperature of PEG (at temperatures of up to 120 °C).

Additionally, these T_d values enhanced with an increasing GNP amount. T_d exhibits a first-order transition, and it can be described by $T_{tr}(T_d) = \Delta H_{tr} / \Delta S_{tr}$, where ΔH_{tr} and ΔS_{tr} are the changes in enthalpy and entropy of the phase transition, respectively [36]; ΔH_{tr} is the dominating parameter influencing T_d . Increasing the GNP concentration increased the thermal energy required to destroy the gels. As a result, ΔH_{tr} and T_d enhanced with increasing GNP content.

Structure

Figure 5 presents the TEM micrographs of GNPs at different magnifications. Multilayered sheet-shaped structures were observed, and the largest and smallest sizes of GNPs were approximately 4 μm and 500 nm, respectively. TEM micrographs of the composite PCMs containing 0, 1, and 4 mass% GNPs at different magnifications are shown in Fig. 6. Three-dimensional networks of DBS nanofibrils with diameters between 10 and 40 nm were observed (Fig. 6 a and b), which is similar to the diameters of the fibrils in organic matrix [29–31]. The fibril sizes were not significantly influenced by increasing in GNP content (Fig. 6 c–f). Further, the dark regions in Fig. 6 (c) and (e) indicate the varying in-plane sizes of the GNPs, and the largest sizes were approximately 4 μm . The schematic drawings of the structure of the prepared PCM are illustrated in Fig. 7.

Heating and cooling performance

Figure 8 demonstrates the DSC curves of the pristine PEG and composite PCMs with 0–8 mass% GNPs. All DSC experiments for each prepared sample were performed at least three times for reproducibility confirmation. The

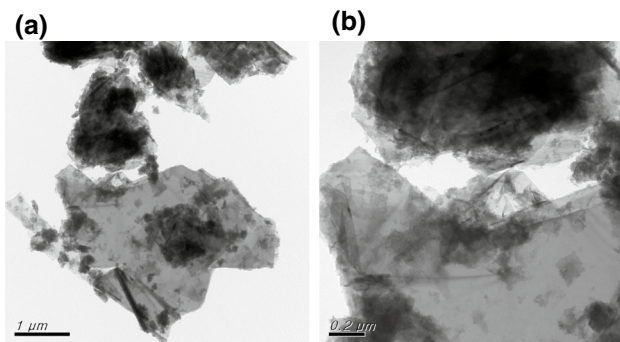


Fig. 5 TEM micrographs of GNPs at different magnifications

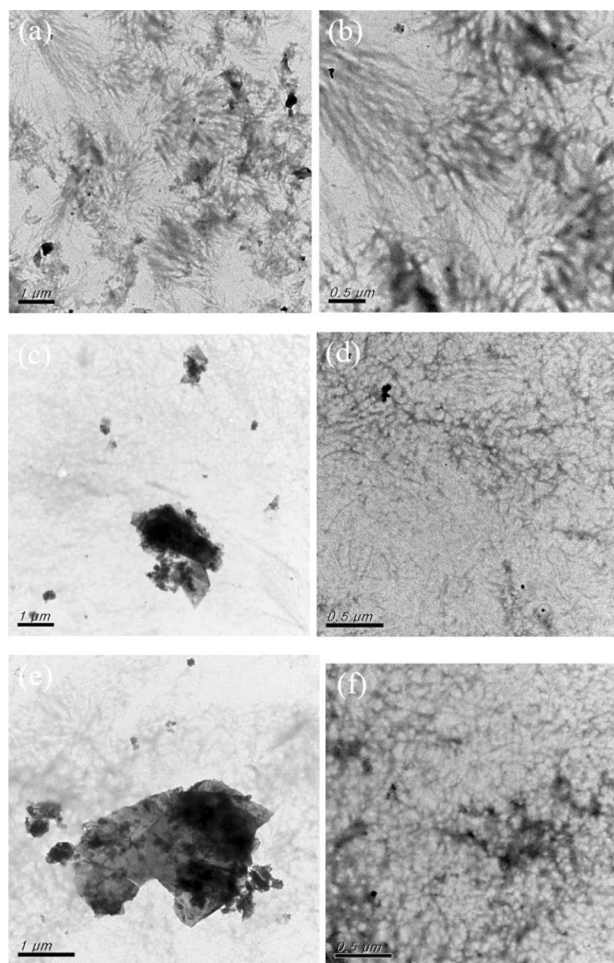


Fig. 6 TEM micrographs at different magnifications of the composite PCMs containing a and b 0, c and d 1, and e and f 4 mass% GNPs

thermal properties of these samples are summarized in Table 1. The freezing and melting temperatures of all samples were around 38 and 60 °C, respectively. These temperatures were not obviously affected with GNPs.

Contrastingly, the latent heats of freezing and melting of the composite PCMs lowered with enhancing GNP amount. For example, the highest latent heat of melting was 185.21/J g^{-1} for the pristine PEG samples (Table 1). With the addition of DBS, the latent heat decreased to 153.44/J g^{-1} . These results suggest that the formation of

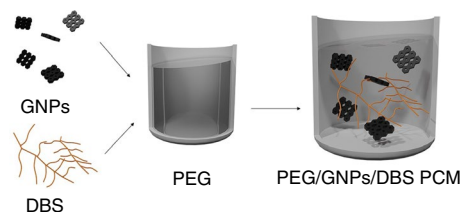


Fig. 7 Schematic drawings of the structure of the prepared PCM

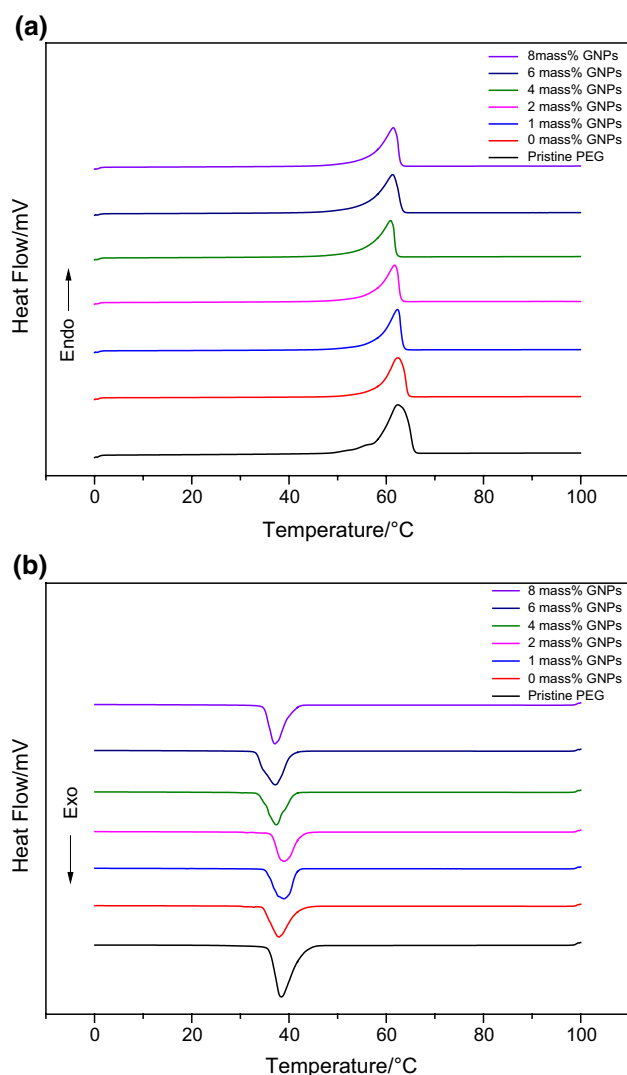


Fig. 8 DSC **a** heating and **b** cooling curves of pristine PEG and composite PCMs with 0–8 mass% GNPs

DBS networks hindered the crystal structures of PEG. Similarly, for samples with varied GNP contents, the latent heat decreased with increasing GNP content. The presence of GNPs disrupted the PEG crystals, resulting in the decrease in the latent heats of the PCMs; the latent heats were above

130 J g⁻¹ for the samples with 0–8 mass% GNPs. The obtained latent heat values are comparable and even higher than those reported for PEG/SiO₂ (113 J g⁻¹) and PEG/SiO₂/Ti₄O₇ (128–139 J g⁻¹) composite PCMs [37, 38].

The DSC curves of composite PCMs with 8 mass% GNPs after different thermal cycles are presented in Fig. 9, and the resulting thermal properties are summarized in Table 2. The samples were analyzed consecutively through 10 and 50 thermal cycles from 20 to 100 °C. The phase transition temperatures and the latent heat of melting and freezing of the PCMs after 10 and 50 thermal cycles were close to those of uncycled composite PCMs. Therefore, these results suggest that the prepared PCMs demonstrated good thermal reliability.

Leakage measurement

The leakage measurements were taken at temperatures larger than the melting temperature of PEG (60 °C). Figure 10 (a) exhibits the plots for leakage percentages versus temperature of the pristine PEG and composite PCMs with 0–8 mass% GNPs. The samples were weighed after maintaining the temperature above the melting temperature of PEG for 30 min. The pristine PEG samples exhibited 94% leakage at 80 °C. Contrastingly, negligible leakage was observed in the PEG/DBS systems until 120 °C. The three-dimensional DBS networks were strong enough to immobilize melted PEG after melting. This implies the samples with DBS remained in the gel state and stabilized the form to prevent leakage. As the temperatures reached 120 °C, the DBS gel networks began to dissolve (T_d ranged from 119 to 127 °C; Fig. 4); the leakage enhanced rapidly after 120 °C.

Figure 10 (b) displays the plot for leakage percentages versus time of the composite PCMs containing 0–8 mass% GNPs at 125 °C, which was close to or higher than the T_d of DBS. Consequently, at 125 °C, the PCMs exhibited the liquids, and the leakage was controlled by the GNPs. The leakage percentage of the composite PCMs with 4 and 8 mass% GNPs lowered with increasing GNP amount. The introduction of GNPs reduced the leakage and stabilized the shape owing to the hydrogen bonding and high specific surface area of the

Table 1 Thermal data of the pristine PEG and composite PCMs with 0–8 mass% GNPs

Sample	$T_m/^\circ\text{C}$	$\Delta H_m/\text{J g}^{-1}$	$T_c(^\circ\text{C})$	$\Delta H_c/\text{J g}^{-1}$
Pristine PEG	62.42 ± 2.35	185.21 ± 12.23	38.50 ± 1.25	-173.94 ± 11.58
0 mass% GNPs	61.76 ± 2.73	153.44 ± 11.87	37.71 ± 1.21	-147.89 ± 10.26
1 mass% GNPs	61.59 ± 1.65	149.58 ± 10.01	38.80 ± 1.58	-143.27 ± 11.74
2 mass% GNPs	61.08 ± 2.97	143.77 ± 8.514	38.90 ± 2.16	-139.13 ± 10.97
4 mass% GNPs	60.24 ± 2.32	137.91 ± 10.13	37.21 ± 1.97	-132.06 ± 10.14
6 mass% GNPs	60.67 ± 3.11	133.93 ± 8.532	37.09 ± 1.75	-128.03 ± 9.529
8 mass% GNPs	60.74 ± 2.95	128.53 ± 9.285	37.01 ± 2.01	-124.50 ± 10.88

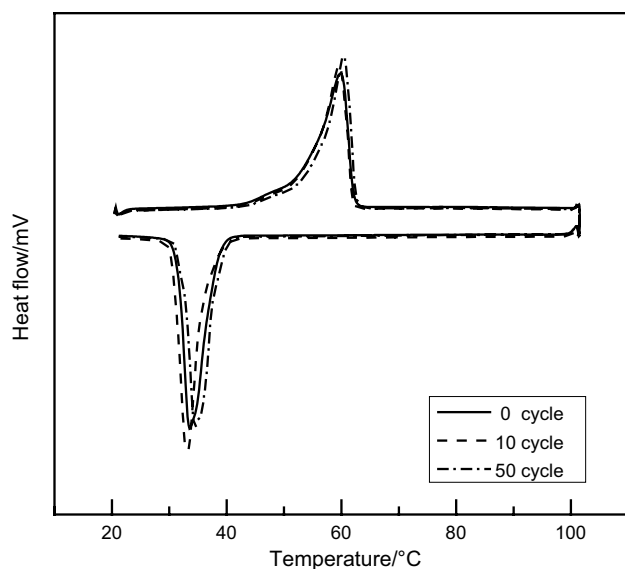


Fig. 9 DSC curves of composite PCMs with 8 mass% GNPs after different thermal cycles

Table 2 Thermal data of the composite PCMs with 8 mass% GNPs

Thermal cycle	$T_m/^\circ\text{C}$	$\Delta H_m/\text{J g}^{-1}$	$T_c/^\circ\text{C}$	$\Delta H_c/\text{J g}^{-1}$
0	59.44 ± 2.08	131.73 ± 10.85	34.13 ± 1.81	-124.50 ± 10.88
10	58.67 ± 1.88	129.84 ± 9.057	35.68 ± 1.85	-127.12 ± 10.18
50	59.91 ± 2.16	133.08 ± 10.39	34.02 ± 1.28	-123.24 ± 11.21

GNPs, which were advantageous for the shape-stabilized PCMs during the solid–liquid transition.

Shape stability

Figure 11 displays the TMA curves of the pristine PEG and composite PCMs with 0–8 mass% GNPs. The dimensions of the pristine PEG samples lowered sharply when the temperature was heated approximately 60 °C. With a further increase in the temperature, the pristine PEG samples completely melted at approximately 65 °C. Although the thickness of the samples with DBS decreased slightly at 60 °C, the thickness of the samples with higher GNP content (4 and 8 mass%) did not change at 60 °C, indicating that the samples with DBS and GNPs retained their shape above 60 °C. These suggest the enhanced shape-stabilized phase change behaviors for the composite PCMs synthesized in this study.

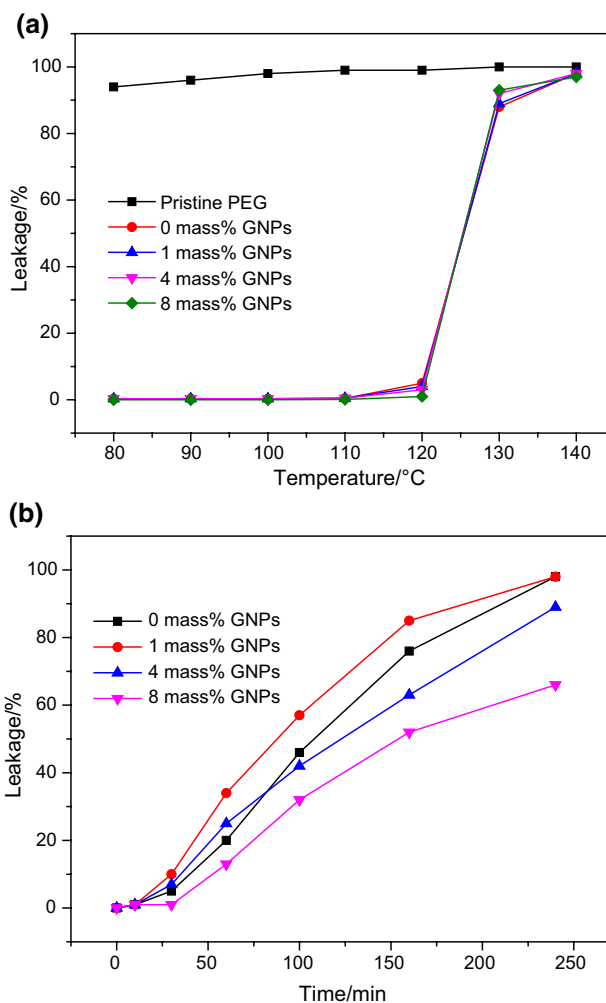


Fig. 10 **a** Leakage percentages versus temperature of the pristine PEG and composite PCMs with 0–8 mass% GNPs and **b** leakage percentages versus time of the composite PCMs containing 0–8 mass% GNPs at 125 °C

Thermal conductivity

Figure 12 presents the thermal conductivity of the composite PCMs containing 0–8 mass% GNPs. The thermal conductivity values of the composite PCMs enhanced with increasing GNP content. The thermal conductivities of the samples with 0, 1, 4, and 8 mass% GNPs were 0.21, 0.25, 0.36, and 0.48 $\text{W/m}^{-1} \text{K}^{-1}$, respectively. The thermal conductivity values of the fabricated PCMs were much larger than those of the pristine PEG. The highest thermal conductivity of the fabricated PCMs was approximately 2.3 times greater than that of PCMs without GNPs. The TMA and thermal conductivity results suggest that GNPs are promising inorganic supporting materials for organic PCMs, which exhibit enhanced shape stabilization and thermal conductivity.

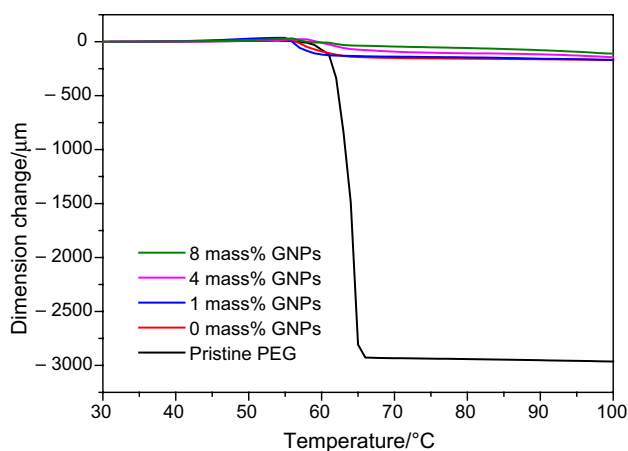


Fig. 11 TMA curves of the pristine PEG and composite PCMs with 0–8 mass% GNPs

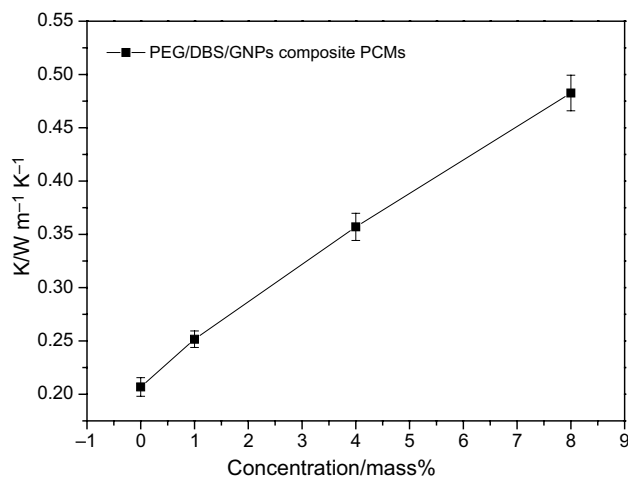


Fig. 12 Thermal conductivity of the composite PCMs containing 0–8 mass% GNPs

Regarding comparisons with previous reports [37–39], the thermal conductivity of the fabricated PCMs was larger than that of PEG/diatomite/CNTs ($0.15\text{--}0.29\text{ W m}^{-1}\text{ K}^{-1}$) and was comparable to that of PEG/diatomite ($0.32\text{--}0.67\text{ W m}^{-1}\text{ K}^{-1}$) and PEG/SiO₂/Cu ($0.29\text{--}0.41\text{ W m}^{-1}\text{ K}^{-1}$) PCMs. Thus, the shape-stabilized PEG PCMs with DBS and GNPs exhibited appropriate thermal conductivity, good latent heat, and excellent shape stabilization.

Conclusions

In the present study, we prepared novel form-stable composite PEG PCMs with small amounts of DBS and GNPs as the supporting materials. Rheological measurements demonstrated that the DBS gels formed after the melting temperature of PEG, implying that these composite PCMs retained their masses and shapes during the phase transition. The DBS gel dissolution temperatures ranged between 119 and 127 °C, which were larger than the PEG melting temperature. The DBS nanofibrillar network, measuring 10–40 nm in diameter, can capture the majority of the melted PCMs to prevent leakage. DSC analysis implies the latent heats of the composite PCMs were higher than 130 J.g^{-1} . TMA results indicate the dimensions of the composite PCMs remain unchanged for the samples with DBS and GNPs, suggesting the excellent form-stable behaviors. Furthermore, the thermal conductivities of the composite PCMs increased significantly with increasing GNP content.

Acknowledgements The authors are thankful to the Ministry of Science and Technology of Taiwan for financial assistance.

References

- Ghoghaei MS, Mahmoudian A, Mohammadi O, Shafii MB, Mosleh HJ, Zandieh M, Ahmadi MH. A review on the applications of micro-/nano-encapsulated phase change material slurry in heat transfer and thermal storage systems. *J Therm Anal Calorim.* 2021;145:1245–68.
- Raj CR, Suresh S, Bhavsar RR, Singh VK. Recent developments in thermo-physical property enhancement and applications of solid solid phase change materials. *J Therm Anal Calorim.* 2020;139:3023–49.
- Xu B, Li P, Chan C. Application of phase change materials for thermal energy storage in concentrated solar thermal power plants: A review to recent developments. *Appl Energy.* 2015;160:286–307.
- Sundararajan S, Samui AB, Kulkarni PS. Versatility of polyethylene glycol (PEG) in designing solid-solid phase change materials (PCMs) for thermal management and their application to innovative technologies. *J Mater Chem A.* 2017;5:18379–96.
- Kousksou T, Bruel P, Jamil A, Rhafikid TE, Zeraouli Y. Energy storage: Applications and challenges. *Sol Energ Mat Sol C.* 2014;120:59–80.
- Omara AAM, Abuelnuor AAA, Mohammed HA, Khiadani M. Phase change materials (PCMs) for improving solar still productivity: a review. *J Therm Anal Calorim.* 2020;139:1585–617.
- Lin Y, Jia Y, Alva G, Fang G. Review on thermal conductivity enhancement, thermal properties and applications of phase change materials in thermal energy storage. *Renew Sust Energ Rev.* 2018;82:2730–42.
- Lin Y, Alva G, Fang G. Review on thermal performances and applications of thermal energy storage systems with inorganic phase change materials. *Energy.* 2018;165:658–708.
- Fang GY, Li H, Chen Z, Liu X. Preparation and properties of palmitic acid/SiO₂ composites with flame retardant as thermal energy storage materials. *Sol Energ Mater Sol C.* 2011;95:1875–81.

10. Sundararajan S, Samui AB, Kulkarni PS. Interpenetrating phase change polymer networks based on crosslinked polyethylene glycol and poly(hydroxyethyl methacrylate). *Sol Energy Mater Sol C*. 2016;149:266–74.
11. Meng QH, Hu JL. A poly(ethyleneglycol)-based smart phase change material. *Sol Energy Mater Sol C*. 2008;92:1260–8.
12. Zalba B, Marin JM, Cabeza LF, Mehling H. Review on thermal energy storage with phase change: materials, heat transfer analysis and applications. *Appl Therm Eng*. 2003;23:251–83.
13. Belessiotis GV, Papadokostaki KG, Favvas EP. Preparation and investigation of distinct and shape stable paraffin/SiO₂ composite PCM nanospheres. *Energy Convers Manage*. 2018;168:382–94.
14. Hasanabadi S, Sadrameli SM, Sami S. Preparation, characterization and thermal properties of surface-modified expanded perlite/paraffin as a form-stable phase change composite in concrete. *J Therm Anal Calorim*. 2021;144:61–9.
15. Pramothraj M, Santosh R, Swaminathan MR, Kumaresan G. Study of effect of Al and Cu microparticles dispersed in D-Mannitol PCM for effective solar thermal energy storage. *J Therm Anal Calorim*. 2020;139:895–904.
16. Trivedi GVN, Parameshwaran R. Microencapsulated phase change material suspensions for cool thermal energy storage. *Mater Chem Phys*. 2020;242: 122519.
17. Qian T, Li J, Min X, Guan W, Deng Y, Ning L. Enhanced thermal conductivity of PEG/diatomite shape-stabilized phase change materials with Ag nanoparticles for thermal energy storage. *J Mater Chem A*. 2015;3:8526–36.
18. Li Y, Li J, Deng Y, Guan W, Wang X, Qian T. Preparation of paraffin/porous TiO₂ foams with enhanced thermal conductivity as PCM, by covering the TiO₂ surface with a carbon layer. *Appl Energy*. 2016;171:37–45.
19. Mochane MJ, Mokhena TC, Motaung TE, Linganisio LZ. Shape-stabilized phase change materials of polyolefin/wax blends and their composites. *J Therm Anal Calorim*. 2020;139:2951–63.
20. Guan W, Li J, Qian T, Wang X, Deng Y. Preparation of paraffin/expanded vermiculite with enhanced thermal conductivity by implanting network carbon in vermiculite layers. *Chem Eng J*. 2015;277:56–63.
21. Mehrali M, Latibari ST, Mahlia Mehrali M. HSC. Preparation and properties of highly conductive palmitic acid/graphene oxide composites as thermal energy storage materials. *Energy*. 2013;58:628–34.
22. Mehrali M, Latibari ST, Mehrali M, Mahlia TMI, Metselaar HSC, Naghavi MS, Sadeghinezhad E, Akhiani AR. Preparation and characterization of palmitic acid/graphene nanoplatelets composite with remarkable thermal conductivity as a novel shape-stabilized phase change material. *Appl Therm Eng*. 2013;61:633–40.
23. Yang J, Tang L-S, Bao R-Y, Bai L, Liu Z-Y, Yang W, Xie B-H, Yang M-B. Largely enhanced thermal conductivity of poly(ethylene glycol)/boron nitride composite phase change materials for solar-thermal-electric energy conversion and storage with very low content of graphene nanoplatelets. *Chem Eng J*. 2017;315:481–90.
24. Lin Y, Cong R, Chen Y, Fang G. Thermal properties and characterization of palmitic acid/nano silicon dioxide/graphene nanoplatelet for thermal energy storage. *Int J Energy Res*. 2020;44:5621–33.
25. Chen H, Xuan J, Deng Q, Gao Y. WOOD/PCM composite with enhanced energy storage density and anisotropic thermal conductivity. *Prog Nat Sci: Mater Int*. 2022;32:191–5.
26. Chen C, Liu W, Wang H, Peng K. Synthesis and performances of novel solid–solid phase change materials with hexahydroxy compounds for thermal energy storage. *Appl Energy*. 2015;152:198–206.
27. Zhou R, Ming Z, He J, Ding Y, Jiang J. Effect of magnesium hydroxide and aluminum hydroxide on the thermal stability, latent heat and flammability properties of Paraffin/HDPE phase change blends. *Polymers*. 2020;12:180.
28. Su W, Zhou T, Li Y, Lv Y. Development of microencapsulated phase change material with poly (methyl methacrylate) shell for thermal energy storage. *Energy Procedia*. 2019;158:4483–8.
29. Lai W-C, Lee Y-C. Self-assembly behavior of gels composed of dibenzylidene sorbitol derivatives and poly(ethylene glycol). *RSC Adv*. 2016;6:98042–51.
30. Olles JR, Slavik P, Whitelaw NK. Self-assembled gels formed in deep eutectic solvents: Supramolecular eutectogels with high ionic conductivities. *Angew Chem Int Ed*. 2019;58:4173–8.
31. Steck K, Stubenrauch C. Gelling lyotropic liquid crystals with the organogelator 1,3:2,4-dibenzylidene-d-sorbitol part I: phase studies and sol-gel transitions. *Langmuir*. 2019;35:17132–41.
32. Niu L, Bai G, Song J. 1,3:2,4-di-(3,4-dimethyl)benzylidene sorbitol organogels used as phase change materials: solvent effects on structure, leakage and thermal performance. *RSC Adv*. 2015;5:21733–9.
33. Lai W-C, Chang C-W, Hsueh C-Y. Shape-stabilized poly(ethylene glycol) phase change materials with self-assembled network scaffolds for thermal energy storage. *Polymer*. 2021;213: 123196.
34. De Gracia A, Rincón L, Castell A, Jiménez M, Boer D, Medrano M, Cabeza LF. Life cycle assessment of the inclusion of phase change materials (PCM) in experimental buildings. *Energy Build*. 2010;42:1517–23.
35. Ahmadi A, Ehyaei MA, Doustgani A, Assad MEH, Hmida A, Jamali DH, Kumar R, Li ZX, Razmjoo A. Recent residential applications of low-temperature solar collector. *J Clean Prod*. 2021;279: 123549.
36. Watase M, Nakatani Y, Itagaki H. On the Origin of the Formation and Stability of Physical gels of di-o-benzylidene-d-sorbitol. *J Phys Chem B*. 1999;103:2366–73.
37. Xu T, Chen Q, Zhang Z, Gao X, Huang G. Investigation on the properties of a new type of concrete blocks incorporated with PEG/SiO₂ composite phase change material. *Build Environ*. 2016;104:172–7.
38. Tang B, Wei H, Zhao D, Zhang S. Light-heat conversion and thermal conductivity enhancement of PEG/SiO₂ composite PCM by in situ Ti₄O₇-doping. *Sol Energy Mater Sol C*. 2017;106:183–9.
39. Sari A, Bicer A, Al-Sulaiman FA, Karaipekli A, Tyagi VV. Diatomite/CNTs/PEG composite PCMs with shape-stabilized and improved thermal conductivity: Preparation and thermal energy storage properties. *Energy & Buildings*. 2018;164:166–75.

Publisher's Note Springer Nature remains neutral with regard to jurisdictional claims in published maps and institutional affiliations.

Springer Nature or its licensor (e.g. a society or other partner) holds exclusive rights to this article under a publishing agreement with the author(s) or other rightsholder(s); author self-archiving of the accepted manuscript version of this article is solely governed by the terms of such publishing agreement and applicable law.